A Generic Convex Model for a Chance-Constrained Look-Ahead Economic Dispatch Problem Incorporating an Efficient Wind Power Distribution Modeling

B. Khorramdel, *Student Member IEEE,* A. Zare, *Student Member IEEE,* C. Y. Chung, *Fellow, IEEE,* and P. N. Gavriliadis

***Abstract*— Power systems with high penetration of wind resources must cope with significant uncertainties originated from wind power prediction error. This uncertainty might lead to wind power curtailment and load shedding events in the system as a big challenge. Efficient modeling and incorporation of wind power uncertainty in generation and reserve scheduling can prevent these events. This paper presents a new framework for wind power cumulative distribution function (CDF) modeling and its incorporation in a new chance-constrained economic dispatch (CCED) problem. The proposed CDF modeling uses few moments of wind power random samples. To validly capture the actual features of the wind power distribution such as main mass, high skewness, tails, and especially boundaries from the moments, an efficient moment problem is presented and solved using the beta kernel density representation (BKDR) technique. Importantly, a new polynomial cost function for efficient modeling of wind power misestimation costs is proposed for the CCED problem that eliminates the need for an analytical CDF and enables the use of an accurate piecewise linearization technique. Using this technique, the non-linear CCED problem is converted to a mixed-integer linear programming (MILP)-based problem that is convex with respect to the continuous variables of the problem. Therefore, it is solved via off-the-shelf mathematical programming solvers to reach more optimal results. Numerical simulations using the IEEE 118-bus test system show that compared with conventional approaches, the proposed MILP-based model leads to lower power system total cost, and thereby is suggested for practical applications.**

***Index Terms*— Chance-constrained optimization, mixed-integer linear programming, wind power probability distribution.**

NOMENCLATURE

A. Abbreviations

BKDR	Beta kernel density representation
CCED	Chance-constrained economic dispatch
CCF	Conventional cost function
CCSO	Chance-constrained stochastic optimization
CDF	Cumulative distribution function
CL	Confidence level
CPPs	Conventional power plants
DRCC	Distributionally robust chance constraints
GMM	Gaussian mixture model
GGMM	Generalized gaussian mixture model
MILP	Mixed-integer linear programming
NCF	New cost function
PB	Power bin
PDF	Probability density function
PIs	Prediction intervals
RMSE	Root mean square error
RO	Robust optimization
SSA	Simplified sequentially adaptive
SLP	Sequential linear programming
SO	Stochastic optimization
TVD	Truncated versatile distribution
VMD	Versatile mixture distribution
WFs	Wind farms

B. Functions

$B(\cdot)$	Beta function.
$C_{t,i}^{g}$	Generation cost of unit i at hour t.
$C_{t,i}^{r}$	Reserve cost of unit i at hour t.
C_{t}^{dw}	Direct cost of wind power generation at hour t.
$\widehat{EC}_t^{UP}, \widehat{EC}_t^{LS}, \widehat{EC}_t^{DN}, \widehat{EC}_t^{WC}$	Estimated expected cost for upward (UP) reserve, load shedding (LS), downward (DN) reserve, and wind curtailment (WC) at hour t.
$F(z)$	A typical non-linear function with variable z.
$\hat{f}_t(\cdot), \hat{F}_t(\cdot)$	Estimated PDF and CDF at hour t.
$\hat{F}_t^{-1}(\cdot)$	Inverse of the estimated CDF at hour t.
f_B	Beta kernel function.
F_e	Empirical CDF.
$\kappa(\cdot)$	Kernel function.

C. Parameters

$A_q/A'_q/B_q/B'_q$	Estimated UP reserve/LS/ DN reserve/WC cost coefficients of wind power generation.
CL^{UP}/CL^{DN}	Confidence levels for enough UP/DN reserve.
c_i^{UP}/c_i^{DN}	UP/DN reserve cost coefficients of unit i.
$\underline{h}/\overline{h}$	Lower/upper values of beta kernel bandwidth.
I	Number of beta kernel components.
L_t^b	Base load of system at hour t.
N	Number of sample moments.
N_{PB}, NG, NW	Number of power bins, CPPs, and WFs.
$\underline{P_i}/\overline{P}_i$	Lower /upper limit of generation for unit i.
$\overline{\Delta P}_i^{UP}/\overline{\Delta P}_i^{DN}$	UP/DN maximum ramp limits.
$\overline{r}_i^{UP}/\overline{r}_i^{DN}$	Maximum value of UP/DN reserve for unit i.
μ_n	n^{th} sample moment of a random variable.
Λ	Number of linearization segments.
$\psi_\lambda, m_\lambda, n_\lambda$	Constant parameters of piecewise linearization.
$\gamma^{UP}/\gamma^{LS}/\gamma^{DN}/\gamma^{WC}$	UP reserve/LS/ DN reserve/WC penalty factors for wind power uncertainty.

D. Variables

$\widehat{D}$	Main-mass interval for PDF construction.
h	Bandwidth of beta kernel for PDF construction.
$P_{t,i}$	Scheduled generation of unit i at hour t.
$r_{t,i}^{UP}/r_{t,i}^{DN}$	Scheduled UP/DN reserve of unit i at hour t.
$R_{t,j}^{UP}/R_{t,j}^{DN}$	Scheduled UP/DN reserve for managing the uncertainty of wind farm j at hour t.
υ_i, ζ_i	Parameters of i^{th} beta component.
ω	Total wind power generation random variable.
ω_t	Scheduled total wind power generation at hour t.
$w_{t,j}$	Scheduled generation of wind farm j at hour t.
$w_{r,j}$	Generation capacity of wind farm j.
x_i/p_i	Location/ weight of i^{th} beta component.
$\delta_\lambda/\Delta_\lambda$	Continuous/binary auxiliary variables of piecewise linearization technique.

This work was supported in part by the Natural Sciences and Engineering Research Council (NSERC) of Canada and the Saskatchewan Power Corporation (SaskPower). Benyamin Khorramdel, Alireza Zare, and C. Y. Chung are with the Department of Electrical and Computer Engineering, University of Saskatchewan, Saskatoon, SK S7N 5A9 Canada (e-mail: benyamin.khorramdel@usask.ca; alireza.zare@usask.ca; c.y.chung@usask.ca). P. N. Gavriliadis is with the Department of Naval Architecture and Marine Engineering at the NTUA, Greece. (e-mail: pmath@central.ntua.gr).

E. Matrices & Vectors

$\boldsymbol{C}_{N\times I}$	Beta kernel moments matrix.
H	Bandwidth vector for optimal beta kernel bandwidth selection.
$\boldsymbol{p}, \boldsymbol{\upsilon}, \boldsymbol{\zeta}$	PDF reconstruction vectors for a typical PB.
$\mathbf{P}, \mathbf{\Upsilon}, \mathbf{Z}$	PDF reconstruction matrices for all PBs.
$\boldsymbol{\mu}$	Moment vector of a random sample.

I. Introduction

A. Motivation

THE increasing penetration of uncertain wind power in overall generation around the world can adversely affect the operation, flexibility, and security of large-scale power systems in terms of reserve depletion, transmission line overloading, incremental cost of total generation, etc. [1]. Accurate wind power generation uncertainty modeling should be accomplished as the first step to handle the uncertainty in power systems [2]-[11]. In the second step, optimal reserve and generation scheduling in a look-ahead economic dispatch (ED) problem should be carried out using an efficient stochastic methodology. Chance-constrained ED (CCED) is one such efficient stochastic methodology for uncertainty management [2]-[5].

Because the conventional cost function (CCF) in the CCED problem includes the expected values of wind power overestimation and underestimation costs expressed by a non-linear and non-convex structure, it is not efficient to solve the CCED problem in a conventional optimization framework. In addition, parametric distribution models containing closed forms for cumulative distribution functions (CDFs) are usually used for wind power [2]-[7], [9], [10]. This structure of CCF prevents power system operators from using more accurate distribution models (e.g., non-parametric models) and efficient optimization algorithms such as mixed-integer linear programming (MILP). Therefore, sequential linear programming (SLP) based on Taylor series expansion is often used as an optimization approach for the CCED problem [2]-[5]. The main motivation of this paper is to propose a generic convex model that is convex with respect to the continuous variables of the problem. Also, it is adaptable to both parametric and non-parametric wind power distribution models and can provide the opportunity to formulate the CCED model like an MILP model while a finite convergence to a global optimal solution for the linearized model is guaranteed.

B. Literature Review and Challenges

Wind power distribution modeling is the cornerstone of overall uncertainty modeling in power systems [8]. Recent studies have proposed parametric probability density functions (PDFs) (e.g., Cauchy [6], Weibull, hyperbolic [7], Gaussian [9], and beta [10]) for wind power generation. In [6], a more flexible and complex distribution, i.e., the Levy α-stable distribution, is also proposed for probabilistic reserve sizing in power systems. Efficient versatile and truncated versatile distributions (TVD) for wind power forecast error are proposed and implemented in a look-ahead stochastic ED in [2], [3]. Conditional wind power forecast error modeling is presented in [8] using a Gaussian copula function for generation scheduling. Alternatively, a Gaussian mixture model (GMM) and a versatile mixture distribution (VMD) are adopted in [4], [5], to represent more accurate wind power distribution models. However, the constructed distributions might show boundary effects because Gaussian and versatile components are not bounded between 0 and 1 p.u. In recent researches, a generalized gaussian mixture model (GGMM) is proposed by [12], [13] for statistical representation and probabilistic forecasting of wind power ramps with especial features like duration, rate, and magnitude. In [11], the Copula Theory is used as an efficient approach to model the dependency structure among wind resources. It uses dependent discrete convolution to obtain the distribution of aggregate wind power in high-dimensional cases. Although dependency structure modeling is important, it is a complex process and is not in the main scope of this paper for overall uncertainty modeling. To deal with the uncertainty of wind power in real-world power system applications, many researchers have proposed different methodologies. Stochastic optimization (SO) is proposed for look-ahead ED in [14]-[16] to

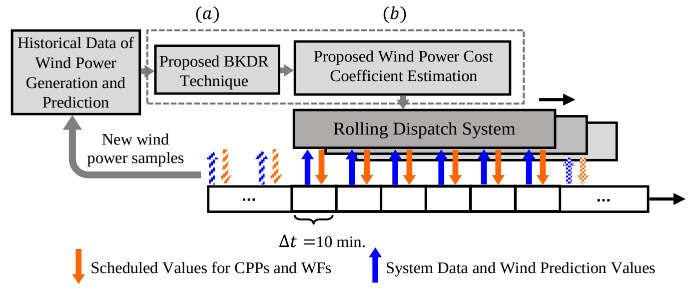

Fig. 1. Overview of the economic dispatch model with the proposed building blocks: (a) BKDR block and (b) wind power cost coefficient estimation block.

manage the uncertainty of renewable energy resources. In SO, several scenarios are extracted from a predetermined probability distribution to consider the possible values of uncertain variables. However, the optimal solution and computational efficiency strongly depend on the number of scenarios and the corresponding probabilities. In [2]-[5], [17], [18], chance-constrained SO (CCSO) is used as a more efficient method by adjusting a predefined level of risk. In this method, accurate distribution models for wind power sources are required to preserve the security of the system with a certain probability level. In [19]-[24] distributionally robust chance-constrained (DRCC) optimization is used, where instead of accurately estimating the wind power probability distribution, a moment-based ambiguity set is defined to cover a family of distributions for uncertainty sources. It can be used in diverse areas such as distribution system planning [19], AC optimal power flow [20], [22]-[23], and energy and reserve dispatch [21]. The keen readers are referred to [24] for mathematical details of DRCC. Robust optimization (RO) as an alternative method that improves the security of the system allows wind power to vary in a given uncertainty range [25]-[27]. However, RO leads to an overly conservative solution because it minimizes the cost of the worst-case scenario. Interval optimization (IO) uses prediction intervals (PIs) and central prediction point to minimize the system operating cost. Compared to CCSO and RO, IO is respectively more conservative and less precise [17], [18], [25]-[28]. In [29], a two-stage optimization process is proposed for battery energy storage capacity for alleviating wind curtailment in a second-order cone programming framework while wind power is modeled by lower and upper intervals. Considering large intra-interval variations of wind power, an intra-interval security dispatch is proposed in [30] to provide a trade-off between economics and security. A strategic reserve purchasing is proposed in [31] to mitigate wind power uncertainty in a real time market and avoid a predetermined penalty for wind power producers (WPPs). In [32], a convex model is proposed for a risk-based unit-commitment that considers wind power uncertainty to manage wind curtailment, load shedding, and line overflow. This paper focuses on CCSO technique for wind power uncertainty management. Based on the literature, the approaches utilized in CCED have used approximate calculations for partial derivatives of the CCF, which might lead to a non-optimal solution [2]-[5]. The abovementioned methodologies for wind power uncertainty modeling and handling in ED problems have their own merits and demerits. The literature, however, lacks an efficient CCED model for simultaneous incorporation of non-parametric distribution models and highly accurate linearization techniques for the cost function. Fig.1 shows an overview of the proposed MILP-based CCED model in this study where the building blocks (a) and (b), as the main novelty of this study, are proposed for an efficient rolling dispatch system. All details of each block are explained in Section II to Section IV through representation of Algorithm 1, Algorithm 2, Algorithm 3, and the general structure of the proposed framework.

C. Contribution

This paper proposes an efficient CCED model and makes the following contributions:

1) An efficient methodology for construction of a new cost function (NCF) is proposed for nonlinear CCED models by which power system operators can use parametric and non-parametric distribution models for wind power.

2) Because of the proposed NCF, a highly accurate linearization technique, i.e., piecewise linearization, can be used to convert the non-linear CCED into an efficient MILP-based model.
3) For the first time, an efficient wind power distribution modeling is proposed using finite sample moments (e.g., 10 to 20) and the beta kernel density representation (BKDR) technique.
4) Because the BKDR technique represents the target distribution using several beta components with restricted parameters' range, it avoids boundary effects while capturing certain features of wind power distribution without reflecting overfitting problem.

D. *Organization*

This paper is organized as follows. In Section II, a new approach for wind power distribution modeling is proposed based on the information provided by several sample moments. Section III and IV present the CCED model and the challenges along with the solution methodology, respectively. Comprehensive simulation results are presented in Section V. Finally, Section VI concludes the paper.

II. Wind Power Distribution Modeling Using the Beta Kernel Density Representation Technique

The reconstruction of a probability distribution $f(x)$ using a limited number of moment data μ_n is called the truncated moment problem first proposed by *Stieltjes* and stated as follows [33].

$$\mu_n = \int x^n f(x)\, dx \quad , \quad n = 0,1,2,\dots,N \tag{1}$$

The question is how to use the information available in μ_n to recover the corresponding target function $f(x)$ with high accuracy. If the target PDF $f(x)$ is bounded in interval $x \in [a,b]$, the truncated *Hausdorff* moment problem is realized [34]. To obtain a satisfactory solution to this problem, two steps should be followed. First, an appropriate representation methodology, i.e., kernel density representation (KDR), for the function to be recovered should be chosen. Second, some important features or *a priori* knowledge about the target PDF $f(x)$, such as boundary conditions, tail behavior, modality information, and the main-mass interval, need to be determined to improve the solution [34]. For a truncated *Hausdorff* moment problem, it suffices to determine the main-mass interval referred to as $\widehat{D}$.

A. *KDR-Based Wind Power PDF Representation*

KDR is a parametric representation of PDF $f(x)$ by means of a weighted sum of known non-negative kernel density functions (KDFs), as shown in (2) [33], [34].

$$\hat{f}(x;\boldsymbol{p}) = \sum_{i=1}^{I} p_i\, \kappa(x; x_i, h) \qquad x \in [0,1] \tag{2}$$

$$\sum_{i=1}^{I} p_i = 1 \quad , \quad p_i \geq 0 \quad , \quad \boldsymbol{p} = [p_1, \dots, p_I]^{\mathrm{T}} \tag{3}$$

Bandwidth parameter h, which controls the smoothness of the overall fit, can be determined either from a predetermined optimal range or by minimizing the estimated error of the KDR model as it is proposed in this work. Equation (2) means that an unknown density function $f(x)$ can be represented by I kernels placed at uniformly distributed locations x_i of the sample space [0,1], where p_i measures the contribution of the i^{th} kernel to the overall density evaluation and should meet the constraints in (3). According to (2), the KDF $\kappa(\cdot)$, the kernel weights p_i, the kernel locations x_i, and bandwidth h should be optimally determined to efficiently reconstruct $f(x)$. The optimal values of parameters p_i, x_i, and , h are obtained through minimizing a performance criterion, e.g., $\|\hat{f} - f\|^2$. Also, instead of using the whole interval [0,1] in (2), a main-mass interval, e.g., $\widehat{D}$, can be estimated by which the performance of the proposed technique is improved. The details of each part are provided in sections II.B, II.C, and II.D, respectively.

B. *A Proper Choice for KDF: Beta Distribution*

For $x \in [0,1]$, the beta PDF with two main parameters (υ, ζ) expressed by (4) is an efficient choice for the KDR process because of four main advantages expressed as follows: (i) it is bounded between 0 and 1 like normalized wind power distribution; thus, by summation of several beta distributions over the range [0,1] a bona fide PDF is obtained without occurring boundary effects; (ii) the set of beta parameters (υ_i, ζ_i) is easily related to the set of location and bandwidth parameters (x_i, h)

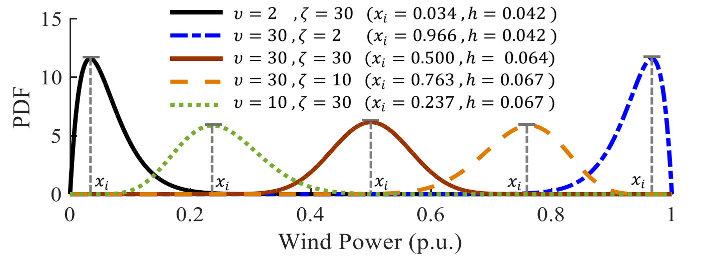

Fig. 2. Illustration of several beta distribution over the range [0,1].

using a closed form (i.e., algebraic system (6)-(7)); (iii) there is a simple function by which the moments of beta distribution can be calculated (i.e., equation (9)); (iv) the flexible shape of the beta distribution symmetrically changes so that it coincides with the skewness of wind power PDF from the lower boundary region to the upper boundary region [10]. Thus, according to (2), the target PDF, $f(x)$, can be approximated by (5). To calculate the parameters υ_i and ζ_i, a natural choice is to use mode and variance expressions of f_B in (6)-(7). Thus, for a given set of values (x_i, h), the parameters (υ_i, ζ_i) are obtained by solving the algebraic system (6)-(7). Fig.2 shows beta distributions with five sets of parameters (υ_i, ζ_i) over the range [0,1].

$$\kappa(x; x_i, h) = f_B(x; \upsilon, \zeta) = \frac{1}{B(\upsilon,\zeta)}\, x^{(\upsilon-1)}(1-x)^{(\zeta-1)} \tag{4}$$

$$\hat{f}(x; \boldsymbol{p}, \boldsymbol{\upsilon}, \boldsymbol{\zeta}) = \sum_{i=1}^{I} \frac{p_i}{B(\upsilon_i,\zeta_i)}\, x^{(\upsilon_i-1)}(1-x)^{(\zeta_i-1)} \tag{5}$$

$$x_i = mode\big(f_B(x; \upsilon_i, \zeta_i)\big) = \frac{\upsilon_i - 1}{\upsilon_i + \zeta_i - 2} \tag{6}$$

$$h^2 = variance\big(f_B(x; \upsilon_i, \zeta_i)\big) = \frac{\upsilon_i\, \zeta_i}{(\upsilon_i+\zeta_i)^2(\upsilon_i+\zeta_i+1)} \tag{7}$$

C. *Optimal Calculation of KDF Weights*

Given a finite number of sample moments $\boldsymbol{\mu} = [\mu_1, \dots, \mu_N]^{\mathrm{T}}$ of an unknown target PDF $f(x)$, I locations on the sample space [0,1] $(I \leq N)$, and bandwidth value h, the weights p_i are calculated by solving the simple minimization problem (8). For the numerical solution of (8), the function *lsqnonneg* of the MATLAB optimization package is employed. The matrix $\boldsymbol{C}_{N\times I}$, which contains N moments of the beta kernel on each location, is obtained by (9) [34]. Therefore, the set of (υ_i, ζ_i) or the locations x_i and bandwidth h should be optimally selected to achieve an optimal solution for (8).

$$\hat{\boldsymbol{p}} = \arg\min_{p_i} \frac{1}{2}\|\boldsymbol{\mu} - \boldsymbol{C}\boldsymbol{p}\|^2 \qquad \text{s.t. (3)} \tag{8}$$

$$\boldsymbol{C}_{n,i} = \int_0^1 x^n f_B(x; \upsilon_i, \zeta_i)\, dx = \prod_{s=0}^{n-1} \frac{\upsilon_i + s}{\upsilon_i + \zeta_i + s} \tag{9}$$

$$n = 0,1,\dots,N \quad , \quad i = 1,2,\dots,I$$

$$RMSE = \left[\frac{1}{N_s}\sum_{i=1}^{N_s}\big(\hat{F}(x_i) - F_e(x_i)\big)^2\right]^{1/2} \tag{10}$$

D. *Optimal Parameters of the Beta KDF*

Simulations show that kernel locations x_i and bandwidth h have a sizable impact on the quality of the overall estimation. It is much easier to find the optimal set (x_i, h) than (υ_i, ζ_i) because the ranges of x_i and h are definite. To find the above-mentioned parameters, a strategy is adopted in this section and shown by Algorithm 1 in Fig. 3. It uses an iterative simplified sequentially adaptive (SSA)algorithm to find optimal locations x_i and a parallel computing-based procedure to find the optimal value of bandwidth h [33]. The basic idea behind the SSA algorithm is to propagate an initial set of kernel locations based on the values of their weights and the distance between successive locations. SSA algorithm is based on two criteria: (i) the death of insignificantly weighted kernels and (ii) the birth of new kernel locations. The first criterion is fulfilled by defining a small threshold value denoted by ε_d. Using this criterion, the kernels with weights smaller than ε_d are removed. The second criterion is met by identifying the kernels with the highest weight and adding two location points nearby. The progressive impoverishment of the resulting KDR model is avoided by considering a small number of iterations k (e.g., $\mathbb{K}$ =5). Algorithm 1 finds the optimal bandwidth h_{opt} through a parallel-computing process based on the minimization of the root mean square error ($RMSE$) in (10).

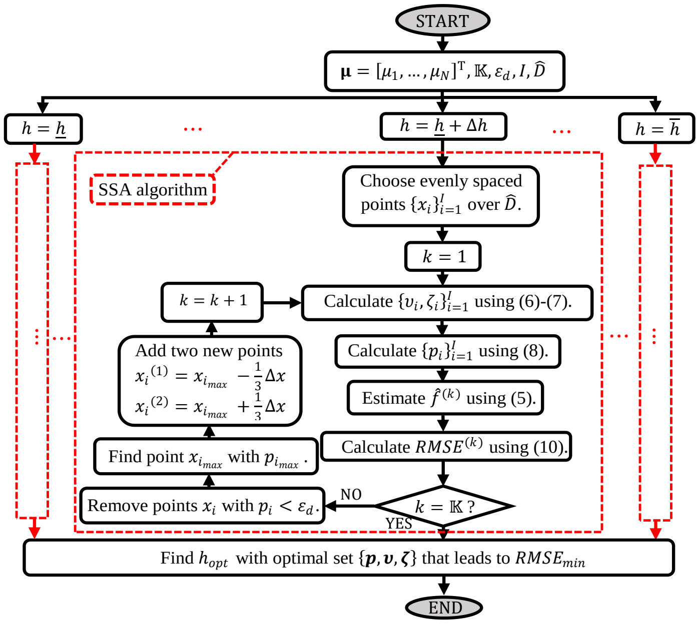

Fig. 3. Flowchart of Algorithm 1 which determines optimal values of beta kernels parameters p_i, x_i, and h where $\Delta x = min\{x_{i_{max}} - x_{i_{max-1}}, x_{i_{max+1}} - x_{i_{max}}\}$.

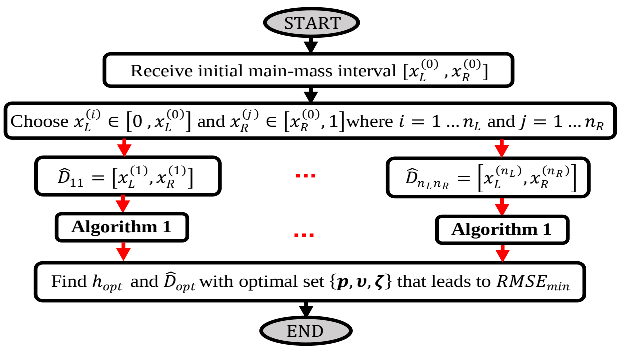

Fig. 4. Flowchart of Algorithm 2 which determines main-mass interval $\widehat{D}$.

The $RMSE_{min}$ is based on CDF estimation and ensures that the estimated CDF contains existing features of the empirical CDF. The $RMSE$ minimization procedure is very fast and simple. Suppose h lies in the range $H = [\underline{h}, \overline{h}]$, and let $h_j, j = 1, \dots, m$ be m evenly spaced points in H. The SSA algorithm is performed for each h_j and iteration k to estimate $\hat{F}$ and compute $RMSE$ to find optimal set $\{\boldsymbol{p}, \boldsymbol{\upsilon}, \boldsymbol{\zeta}\}$. In order to avoid PDFs with many peaks and valleys as an over-fitted modeling, three input parameters I, h, and $\mathbb{K}$ in the proposed SSA algorithm are set on reasonable ranges $I \in [5,20]$, $h \in [0.01, 0.10]$, and $\mathbb{K} \in [2,5]$. Therefore, high computational efficiency and accuracy of distribution modeling can be assured without overfitting. As indicated, the overall improvement of the PDF reconstruction procedure is achieved by determining the main-mass interval $\widehat{D}$ in which the beta functions are placed. In this work, instead of setting the main-mass interval to be equal to the support (i.e., $\widehat{D} = [0,1]$) and varying the number of location points I based on some criteria, an initial main-mass interval $[x_L^{(0)}, x_R^{(0)}]$ is chosen, then the endpoints of the main-mass interval change. In this way, a set of intervals are obtained, and Algorithm 1 can be applied to each interval. A reasonable and simple choice for endpoints $[x_L^{(0)}, x_R^{(0)}]$ that covers the main part of the probability mass is based on the empirical PDF. The main steps of this procedure are given by Algorithm 2 in which Algorithm 1 is the main part as shown in Fig. 4.

E. Proposed Conditional Modeling of Wind Power CDF

As the level of wind power uncertainty greatly depends on the forecast value, the wind power PDF has a conditional relationship with the wind power forecast value [7], [8]. In this section, the conditional model of wind power PDF is presented based on the proposed wind power distribution modeling. However, the performance of the proposed probability distribution modeling does not depend on the deterministic prediction accuracy since the proposed model tunes the range of input parameters I, h, $\widehat{D}$, and $\mathbb{K}$ by pre-processing of received actual and predicted time series. For given forecast value $\widehat{\omega}_t$, the wind power PDF is specified using (11) with predetermined optimal sets of $\boldsymbol{p}$, $\boldsymbol{\upsilon}$, and $\boldsymbol{\zeta}$. To assign a certain set of $\boldsymbol{p}$, $\boldsymbol{\upsilon}$, and $\boldsymbol{\zeta}$ to forecast value $\widehat{\omega}_t$, the forecast range [0,1] p.u. is first divided into several equally sized power bins (PBs). N_{PB} depends on the length of the wind power time series under study, which usually equals to 20 if there are sufficient samples (i.e., X_i) inside each PB. Then, using the wind power samples inside each PB, the sample moments (i.e., μ_n) of wind power are calculated via (12). Finally, using Algorithm 2, the optimal sets $\mathbf{P}$, $\mathbf{\Upsilon}$, and $\mathbf{Z}$, expressed by (13), are obtained for the related time series. Therefore, different PBs have different sets of $\boldsymbol{p}$, $\boldsymbol{\upsilon}$, and $\boldsymbol{\zeta}$ that lead to PDFs with diverse features. The matrices $\{\mathbf{P}, \mathbf{\Upsilon}, \mathbf{Z}\}$ can be updated weekly. The proposed wind power CDF modeling might be run every day, every week, etc. whenever enough new wind power samples are available for updating the inputs.

In this paper, for the sake of simplicity, the time series of real and predicted wind power are supposed to have 10-min resolution with 10-min prediction horizon. However, for conditional PDF modeling, the evolution of estimated PDFs depends on the prediction horizon and resolution. The prediction horizon and resolution of the time series under study should be consistent with the power system generation and reserve dispatch because, for example, the PDF of wind power looking 10-min ahead is different from 1-hour ahead. If the dispatch system is run every hour with 10-min resolution, the prediction horizon of historical data can be one hour with the same resolution. It is worth noting that, without loss of generality, the proposed conditional PDF modeling can be done for various prediction horizons and resolutions.

$$f(x|\widehat{\omega}_t) = f(x|\boldsymbol{p}, \boldsymbol{\upsilon}, \boldsymbol{\zeta}) = \hat{f}(x; \boldsymbol{p}, \boldsymbol{\upsilon}, \boldsymbol{\zeta}) \tag{11}$$

$$\mu_n = \frac{1}{N_s} \sum_{i=1}^{N_s} X_i^n \quad , \quad n = 0,1,2, \dots, N \tag{12}$$

$$\mathbf{P} = \{\boldsymbol{p_k}\}_{k=1}^{N_{PB}} \ , \mathbf{\Upsilon} = \{\boldsymbol{\upsilon_k}\}_{k=1}^{N_{PB}} \ , \mathbf{Z} = \{\boldsymbol{\zeta_k}\}_{k=1}^{N_{PB}} \tag{13}$$

F. Comparisons with Other Distribution Models

To show the superiority of the proposed wind power distribution modeling, a quantitative analysis is provided to compare with TVD, GMM, VMD, and GGMM [3]-[7], [12], [13] using three wind power datasets. **Dataset 1**- Canada's Alberta Electric System Operator (AESO) dataset with 1463 MW capacity (WF1); **Dataset 2**- Canada's Centennial wind farm in Saskatchewan province with 150 MW capacity (WF2); and **Dataset 3**- Spain's Sotavento wind farm with 17 MW capacity (WF3) [36], [37].

This study uses the $RMSE$ index to calculate the closeness of approximate CDF models to actual distributions. Table I shows that the BKDR technique outperforms others by presenting the minimum value of $RMSE$ for the related PB of three different wind farms. However, BKDR and GMM show the same performance for $\{PB_{19}\}$ of WF1, $\{PB_3, PB_{18}\}$ of WF2, and $\{PB_9, PB_{10}, PB_{18}, PB_{20}\}$ of WF3. Importantly, GMM cannot give a reasonable solution for PB_1 of WF2 and WF3. Two datasets WF2+WF3 and WF1+WF2+WF3 are used to demonstrate the performance of BKDR, GGMM, and VMD for aggregate wind power generation in Table II. Because these approaches use approximately the same strategy for distribution modeling, they reflect the same performance for generation levels far from boundaries, and for boundary areas such as PB1, PB19, and PB20, BKDR makes a little difference. A qualitative comparison is shown in Figs. 5 and 6 to have a visual sense of BKDR performance. Fig. 5 shows the CDF of WF1, WF2, and WF3 obtained by TVD and BKDR along with the actual distribution for different levels of generation. Because the CDFs acquired by GMM are very close to those obtained by BKDR, they are not shown in Fig. 5 for the sake of clarity. Fig. 5 shows that the BKDR can follow the variations of actual distributions quite well. Fig. 6 indicates the actual histogram and fitted distribution models for datasets WF2+WF3, WF1+WF2+WF3, and WF1. It is obvious that single-mode Gaussian, beta, and TVD models cannot compete with GMM, VMD, GGMM, and BKDR while the performance of the last three models is quite close to each other. Table III shows the computation time for different distribution models. Compared with other models, the proposed BKDR model

TABLE I
RMSE INDEX FOR DIFFERENT LEVELS OF WIND GENERATION

PB_i	RMSE(%)								
	WF1			WF2			WF3		
	TVD	**GMM**	**BKDR**	**TVD**	**GMM**	**BKDR**	**TVD**	**GMM**	**BKDR**
PB_1	3.50	2.50	**1.67**	2.80	---	**1.06**	1.85	---	**0.83**
PB_2	2.27	0.61	**0.54**	0.81	0.71	**0.63**	0.33	0.28	**0.27**
PB_3	1.58	0.65	**0.63**	0.62	**0.57**	**0.57**	0.28	0.27	**0.25**
PB_9	1.22	0.78	**0.70**	0.84	0.66	**0.32**	0.67	**0.26**	**0.26**
PB_{10}	1.15	0.52	**0.50**	1.05	0.74	**0.70**	0.83	**0.57**	**0.57**
PB_{14}	0.60	0.40	**0.34**	1.21	1.15	**1.14**	0.52	0.50	**0.49**
PB_{15}	0.98	0.68	**0.53**	1.10	0.88	**0.78**	0.60	0.45	**0.42**
PB_{18}	1.15	0.57	**0.46**	1.84	**0.90**	**0.90**	1.17	**0.65**	**0.65**
PB_{19}	1.91	**0.44**	**0.44**	1.56	0.83	**0.69**	1.70	0.79	**0.78**
PB_{20}	1.31	1.00	**0.98**	1.85	0.81	**0.72**	3.87	**1.00**	**1.00**

TABLE II
RMSE INDEX FOR DIFFERENT LEVELS OF AGGREGATE WIND GENERATION

PB_i	RMSE(%)					
	WF2+WF3			WF1+WF2+WF3		
	VMD	**GGMM**	**BKDR**	**VMD**	**GGMM**	**BKDR**
PB_1	0.72	0.70	**0.67**	0.60	**0.58**	**0.58**
PB_3	**0.25**	**0.25**	**0.25**	**0.23**	**0.23**	**0.23**
PB_{15}	**0.33**	**0.33**	0.34	**0.33**	**0.33**	**0.33**
PB_{19}	0.42	**0.40**	**0.40**	0.40	0.39	**0.38**
PB_{20}	0.92	0.92	**0.90**	0.91	0.90	**0.87**

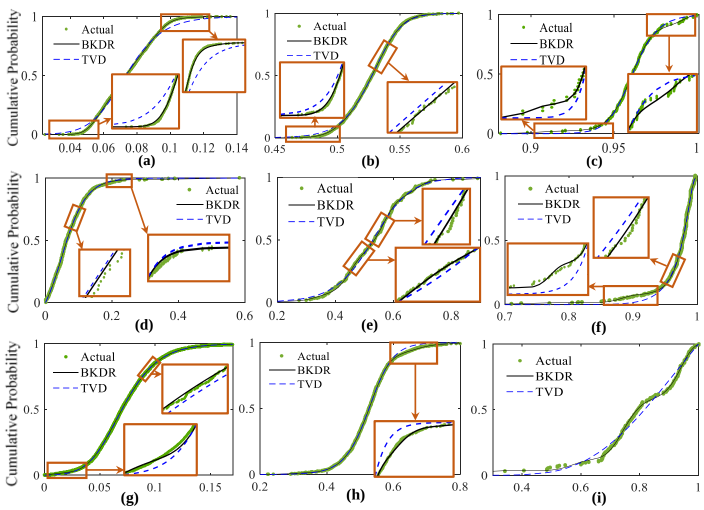

Fig. 5. Actual, BKDR, and TVD fits of the CDF for WF1 (a)-(c), WF2 (d)-(f), and WF3 (g)-(i) for wind power forecast values of 0.05 (a-d-g), 0.5 (b-e-h), and 0.98 (c-f-i) p.u., respectively.

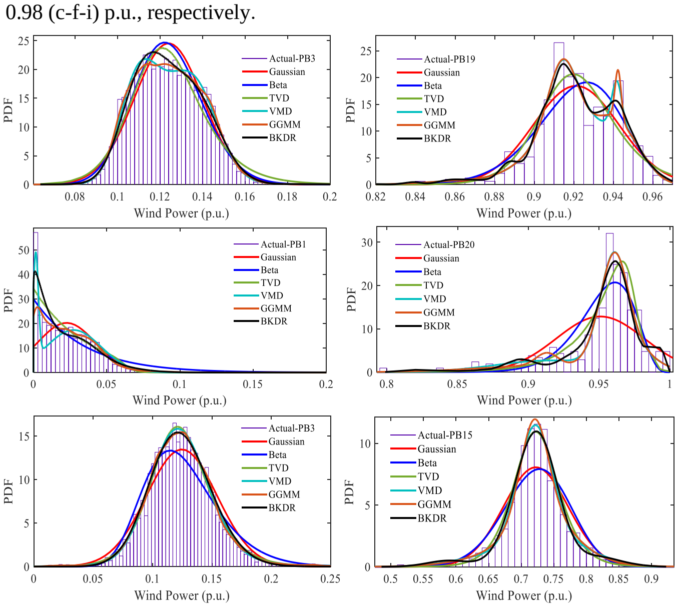

Fig. 6. Comparison of PDFs for WF2+WF3 dataset (upper figures), W1+WF2+WF3 dataset (middle figures), and WF1 dataset (lower figures).

TABLE III
COMPUTATION TIME FOR DIFFERENT DISTRIBUTION MODELS

Distribution Model	Gaussian	Beta	TVD	VMD	GGMM	BKDR
Average Time (sec.)	24.50	26.20	17.30	22.50	21.70	21.30

has a reasonable computation time for real applications in wind power generation modeling.

III. PROPOSED CHANCE-CONSTRAINED ED PROBLEM

A look-ahead ED problem, which affects the online operation of power systems, is a submodule of multiple time-scale coordinated active power control systems. It is performed once per hour to determine the active power output of all generation units over the forthcoming four hours with a time resolution of 10 or 15 minutes [2], [3], [5], [26]. With high penetration of wind generation, a cost function is minimized while satisfying several constraints in a look-ahead CCED problem as an efficient stochastic optimization methodology that allows the uncertainties to be handled by mitigating wind power underestimation and overestimation impacts. In [2], [3], and [5] efficient formulations for generation and reserve scheduling are proposed in look-ahead and real-time CCED models. In the next sections, these formulations are expanded and explained to reach the proposed NCF and MILP-based CCED model.

A. *Cost Function and Constraints of the CCED Problem*

To make decisions under uncertain situations, a classical two-stage stochastic problem is recommended where some of the decisions must be made before the uncertainty is realized (first stage), and then the recourse decisions can be made after the realizations (second stage) [38]. The classical two-stage linear stochastic problems can be formulated as $\min_{x \in X} A^T x + \mathbb{E}[Z(x,\xi)]$ where $x \in \mathbb{R}^n$ is the first-stage decision vector, ξ is the data of the second stage, and $Z(x,\xi)$ is the optimal solution of the second stage defined as $\min_{y} z^T y$ subject to $Bx + Cy \leq D$ where $y \in \mathbb{R}^m$ is the second-stage decision vector and $\xi = (z, B, C, D)$. In this kind of formulation, a "here-and-now" decision should be made for x at the first stage before knowing the realization of uncertain data ξ. At the second stage, after a realization of ξ, another optimization problem should be solved to optimize the decision-making procedure. Therefore, the solution of the second-stage problem is viewed as a recourse action where the term Cy mitigates the inconsistency of $Bx \leq D$, and $z^T y$ would be the cost of this recourse action. If the random variable ξ has a finite support, a linear programming equivalent to the two-stage model can be used as $\min_{x} A^T x + \int Z(x,\xi) f(\xi) d\xi$ which after solving this problem, an optimal solution which can cover all possible scenarios of ξ is found.

In this paper, similarly, the cost function of the stochastic look-ahead ED problem is shown in (14)-(21). The costs related to the uncertainty of wind power generation originate from the overestimation and underestimation of wind power. Fig. 7 shows four main areas of wind power generation uncertainty as well as the actual and fitted distributions for the forecast value $\widehat{\omega}_t = 0.1$ p.u. The main goal of Fig. 7 is to show the main areas of wind power distribution model and their relations with the scheduled value. To mitigate the impact of wind power overestimation, one strategy is to take upward reserve. If the upward reserve does not suffice, a load shedding strategy will be added. Similarly, wind power underestimation is mainly alleviated using downward reserve, and a wind curtailment strategy is added when downward reserve is not adequate. Therefore, wind power overestimation cost equals the expected upward reserve cost EC_t^{UP} with penalty factor γ^{UP} plus the expected load shedding cost EC_t^{LS} with penalty factor γ^{LS} shown in (18) and (19), respectively. Also, wind power underestimation cost equals the expected downward reserve cost EC_t^{DN} with penalty factor γ^{DN} plus the expected wind curtailment cost EC_t^{WC} with penalty factor γ^{WC} expressed by (20) and (21), respectively. Although not all electricity markets apply penalty factors γ^{UP} and γ^{DN} for deviation of wind power generation from the scheduled values, in this paper these penalty factors are considered for generalization of the proposed model [2], [3], [5].

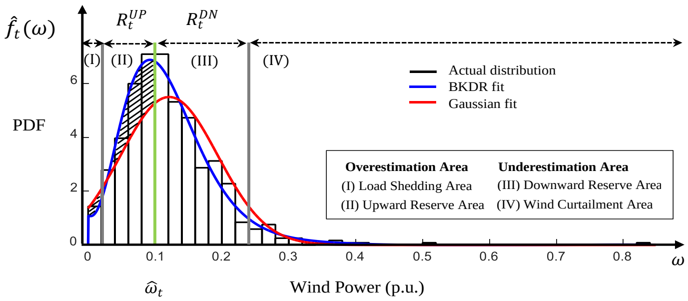

Fig. 7. Illustration of wind power uncertainty and overestimation/underestimation areas for forecast value $\hat{\omega}_t = 0.1$ (p.u.) for PB_3 of WF2.

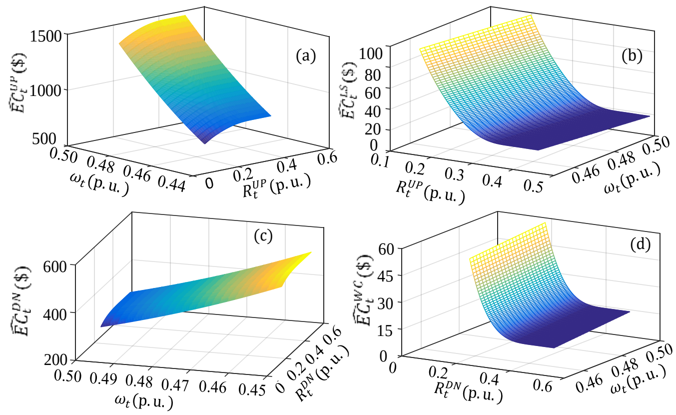

Fig. 8. Illustration of wind power overestimation cost variations ((a) upward reserve cost, (b) load shedding cost) and underestimation cost variations ((c) downward reserve cost, (d) wind curtailment cost) for PB_{10} of WF2.

$$Minimize \ \sum_{t=1}^{T} \Delta t.\left(\sum_{i=1}^{NG} C_{t,i}^{g} + \sum_{i=1}^{NG} C_{t,i}^{r} + C_t^{dw} + EC_t^{UP} + EC_t^{LS} + EC_t^{DN} + EC_t^{WC}\right) \quad (14)$$

$$C_{t,i}^{g} = a_i\left(P_{t,i}{}^{2}\right) + b_i\left(P_{t,i}\right) + c_i \quad \forall t, i \quad (15)$$

$$C_{t,i}^{r} = c_i^{UP}\left(r_{t,i}^{UP}\right) + c_i^{DN}\left(r_{t,i}^{DN}\right), \forall t, i \quad (16)$$

$$C_t^{dw} = d_t(\omega_t) \quad , \forall t \quad (17)$$

$$EC_t^{UP} = \gamma^{UP}\left(\int_{\omega_t - R_t^{UP}}^{\omega_t} (\omega_t - \omega)\hat{f}_t(\omega)d\omega + \int_0^{\omega_t - R_t^{UP}} R_t^{UP} \hat{f}_t(\omega)d\omega\right) \ , \ \forall t \quad (18)$$

$$EC_t^{LS} = \gamma^{LS}\left(\int_0^{\omega_t - R_t^{UP}} \left((\omega_t - R_t^{UP}) - \omega\right)\hat{f}_t(\omega)d\omega\right) \ , \forall t \quad (19)$$

$$EC_t^{DN} = \gamma^{DN}\left(\int_{\omega_t}^{\omega_t + R_t^{DN}} (\omega - \omega_t)\hat{f}_t(\omega)d\omega + \int_{\omega_t + R_t^{DN}}^{\omega_r} R_t^{DN} \hat{f}_t(\omega)d\omega\right) , \ \forall t \quad (20)$$

$$EC_t^{WC} = \gamma^{WC}\left(\int_{\omega_t + R_t^{DN}}^{\omega_r} \left(\omega - (\omega_t + R_t^{DN})\right)\hat{f}_t(\omega)d\omega\right) \ , \forall t \quad (21)$$

s.t.

$$\sum_{i=1}^{NG} P_{t,i} + \omega_t = L_t^b \qquad \forall t \quad (22)$$

$$\sum_{j=1}^{NW} \mathcal{W}_{t,j} = \omega_t \qquad \forall t \quad (23)$$

$$0 \le \mathcal{W}_{t,j} \le \mathcal{W}_{r,j} \qquad \forall t, j \quad (24)$$

$$\begin{cases} \sum_{i=1}^{NG} r_{t,i}^{UP} = R_t^{UP} \\ \sum_{i=1}^{NG} r_{t,i}^{DN} = R_t^{DN} \end{cases} \qquad \forall t \quad (25)$$

$$\begin{cases} 0 \le R_t^{UP} \le \omega_t \\ 0 \le R_t^{DN} \le \ \omega_r - \omega_t \end{cases} \qquad \forall t \quad (26)$$

$$\begin{cases} \mathbb{P}\mathrm{r}\{R_t^{UP} \ge \omega_t - \omega\} \ge CL^{UP} \\ \mathbb{P}\mathrm{r}\{R_t^{DN} \ge \omega - \omega_t\} \ge CL^{DN} \end{cases} \qquad \forall t \quad (27)$$

$$\underline{P}_i + r_{t,i}^{DN} \le P_{t,i} \le \overline{P}_i - r_{t,i}^{UP} \qquad \forall t, i \quad (28)$$

$$\begin{cases} 0 \le r_{t,i}^{UP} \le \overline{r}_i^{UP} \\ 0 \le r_{t,i}^{DN} \le \overline{r}_i^{DN} \end{cases} \qquad \forall t, i \quad (29)$$

$$\begin{cases} P_{t,i} - P_{t-1,i} \le \overline{\Delta P}_i^{UP} \\ P_{t-1,i} - P_{t,i} \le \overline{\Delta P}_i^{DN} \end{cases} \qquad \forall t, i \quad (30)$$

where (22) reflects system's power balance constraints, (23) shows that the summation of WFs' scheduled wind power equals the scheduled aggregate wind power, and (24) defines the range of scheduled WFs' generation. The constraints in (25) show the equality of total CPPs reserves with required reserves for aggregate wind power, and (26)-(27) denote the range of required reserve at each hour. The uncertain random variable of the system shown by ω reflects the possible values of actual wind power generation. The operator $\mathbb{P}\mathrm{r}\{\cdot\}$ in (27) is a probability measure and indicates the chance constraints applied to the upward and downward reserves considered for aggregate wind power. The generation and reserve constraints as well as ramp-rate constraints are represented by (28)-(30). Note that the chance-constrained limits in (27) can be rewritten as (31).

$$\begin{cases} R_t^{UP} \ge \omega_t - \hat{F}_t^{-1}(1 - CL^{UP}) \\ R_t^{DN} \ge \hat{F}_t^{-1}(CL^{DN}) - \omega_t \end{cases} \qquad \forall t \quad (31)$$

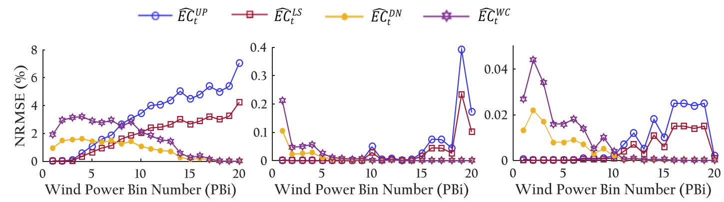

Fig. 9. Fitting error of four parts of the proposed NCF for three different wind farms WF1, WF2, and WF3 from left to right, respectively.

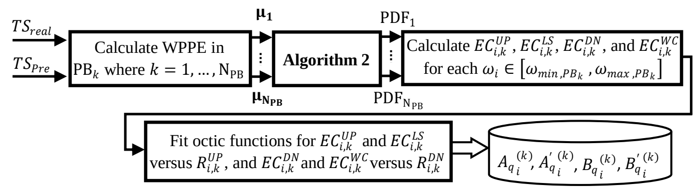

Fig. 10. Structure of Algorithm 3 for wind power cost coefficients estimation.

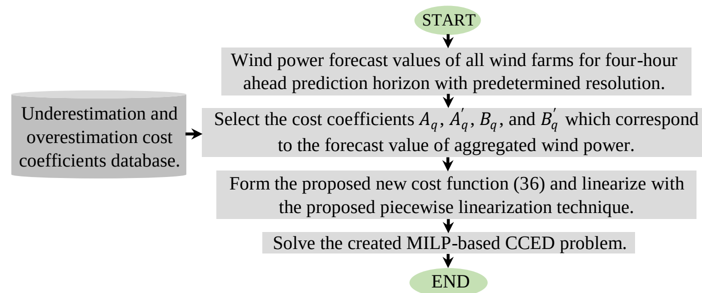

Fig. 11. General structure of the solution algorithm for the proposed MILP-based CCED model.

IV. Challenges and Solutions for CCED Problem

A. Existing Challenges

Regarding the implementation of the CCED problem, there are two main challenges as follows.

1) The distribution model of wind power, shown by $\hat{f}_t(\omega)$, should reflect the main features of the actual distribution such as mode, long tail, high skewness, etc. while avoiding boundary effects. Fig. 7 compares the appropriate BKDR fit (proposed model) and unsuited Gaussian fit and highlights the existing differences in overestimation area with two hatched areas. Considering equations (18)-(19), the difference between the actual and fitted distributions leads to the miscalculation of the upward reserve and the load shedding costs, as will be shown in Section V. Likewise, considering (20)-(21), the existing mismatch in the underestimation area of the probability distribution causes a misjudgment about the downward reserve and wind curtailment costs. As a result, the solutions of the CCED problem might not be optimal if fed by the distribution models such as Gaussian, beta, stable, versatile, etc., that suffer from either boundary effects or low flexibility in terms of showing the above main features [2]-[7], [9], [10]. However, the boundary effects challenge is alleviated using TVD in [3].

2) The most important challenge is that the CCF in (14) contains the non-linear functions (18)-(21) defined by integrals, which makes tackling such an optimization problem difficult. This mainly originates from the dependency of the integral operators' boundaries in (18)-(19) on the pair decision variables $\{R_t^{UP}, \omega_t\}$ and dependency of integral operators' boundaries in (20)-(21) on $\{R_t^{DN}, \omega_t\}$, such that there is not a closed form for the CCED cost function versus the decision variables. Consequently, the partial derivatives of the CCF with respect to these variables (as required for interior-point and SLP optimization techniques) might not be correctly derived. Nevertheless, based on partial derivative formulations in [2]-[5], the boundaries of integrals are ignored, and approximate partial derivatives are proposed for integral functions that might lead to misleading results.

B. Potential Solutions

The first challenge is remediated by the proposed BKDR technique in Section II. The proposed BKDR technique can well estimate the PDF of wind power generation and avoid boundary effect. To address the second challenge, an NCF is explicitly proposed for the CCED problem; specifically, it can be formulated like an MILP model and efficiently solved using standard MILP solvers. To this end, $EC_t^{UP}$and EC_t^{LS} in (18)-(19) are explicitly reformulated with respect to the decision variables R_t^{UP} and ω_t, and $EC_t^{DN}$and EC_t^{WC} in (20)-(21) are rewritten versus R_t^{DN} and ω_t. These reformulated functions are expressed using polynomial functions with degree q $(4 \le q \le 8)$ to accurately model wind power overestimation and underestimation costs. The polynomials are single-variable functions with the variables R_t^{UP} or R_t^{DN}, and just the coefficients depend on variable ω_t. The polynomial fitting procedure is done for every value of wind power over the range [0,1] with a certain resolution. For this procedure, first, suppose ω_t takes on a constant value over PB_k where $k = 1 \dots N_{\mathrm{PB}}$, and the integral operators in (18)-(21) are expanded independently while the main variables R_t^{UP} and R_t^{DN} take on the valid values over the specific ranges defined by (26) and (31). By repeating this procedure for each value of ω_t, the integral-based functions can be represented by few lookup tables. Then, they can be precisely expressed in the form of an octic function with decision variables R_t^{UP} or R_t^{DN}, as shown in (32)-(35) where n=8. Also, the cost coefficients A_q, A'_q, B_q, and B'_q of the octic functions only depend on ω_t, and the hat sign shows that the cost functions are approximate functions. Note, for each value of wind power inside each PB, a separate octic function is fitted. As an example, the fitted cost functions (32)-(35) are shown in Fig. 8 for all wind power values in PB_{10} of WF2 dataset. It shows the nonlinearity and convexity of each function for a certain level of generation; however, it is not guaranteed that the summation of these functions for different generation levels to be a convex function. The fitting error of approximate underestimation and overestimation cost functions are shown in Fig. 9 for WF1 to WF3. The fitting error for wind farms with high generation capacity is more than those with low generation capacity because the non-linearity of the cost functions in (18)-(21) increases proportional to wind farm generation capacity.

$$\widehat{EC}_t^{UP} = \sum_{q=0}^{n} A_q \,.\, (R_t^{UP})^q \tag{32}$$

$$\widehat{EC}_t^{LS} = \sum_{q=0}^{n} A'_q \,.\, (R_t^{UP})^q \tag{33}$$

$$\widehat{EC}_t^{DN} = \sum_{q=0}^{n} B_q \,.\, (R_t^{DN})^q \tag{34}$$

$$\widehat{EC}_t^{WC} = \sum_{q=0}^{n} B'_q \,.\, (R_t^{DN})^q \tag{35}$$

$$NCF = \sum_{t=1}^{T} \Delta t. \left(\sum_{i=1}^{NG} C_{t,i}^{g} + \sum_{i=1}^{NG} C_{t,i}^{r} + C_t^{dw} + \widehat{EC}_t^{UP} + \widehat{EC}_t^{LS} + \widehat{EC}_t^{DN} + \widehat{EC}_t^{WC} \right) \tag{36}$$

The main process of obtaining the proposed NCF in (36) is based on the estimation of cost coefficients A_q, A'_q, B_q, and B'_q as shown by Algorithm 3 in Fig. 10. One of the main building blocks of Algorithm 3 is Algorithm 2 which estimates the wind power PDF of PBs. The estimated cost coefficients for total wind power generation ω_t with a certain resolution over the range [0,1] are stored in a database. In the proposed MILP-based CCED model, the corresponding cost coefficients for each wind power forecast value are chosen from the database, and estimated functions (32)-(35) can be explicitly formed versus decision variables R_t^{UP} and R_t^{DN}. The structure of the proposed MILP-based CCED model is depicted in Fig. 11 where the utilized linearization technique is presented in Section III-C and the detailed solution methodology is presented in Section III-D.

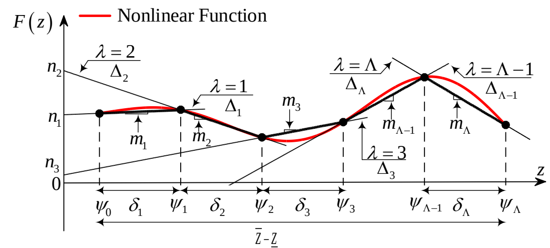

Fig. 12. Piecewise linear approximation of a typical non-linear function.

C. Piecewise Linearization of the Proposed NCF

The CCF is a non-linear function without a closed form that makes achieving the global optimal solution difficult [3]-[5]. Using the proposed reformulation process, an NCF is reproduced to lead to a solution closer to the global solution. To overcome the non-linearity of the proposed NCF, a highly accurate piecewise linearization technique is used [19]. By doing so, the CCED problem is converted to a tractable MILP-based model that can be solved using off-the-shelf mathematical programming solvers such as CPLEX and Gurobi. The non-linearity of the cost function arises from the quadratic function in (15) as well as the proposed octic functions (32)-(35). Let us express each of these non-linear functions as $F(z)$. Using a highly accurate piecewise linearization technique, $F(z)$ can be linearized as (37)-(41), where $\overline{z}$ and $\underline{z}$ represent the upper and lower limits of the variable z, respectively.

$$F(z) = \sum_{\lambda=1}^{\Lambda} (m_\lambda \delta_\lambda + n_\lambda \Delta_\lambda) \tag{37}$$

$$z = \sum_{\lambda=1}^{\Lambda} \delta_\lambda \tag{38}$$

$$\psi_{\lambda-1}\Delta_\lambda \le \delta_\lambda \le \psi_\lambda \Delta_\lambda \;\;, \quad \lambda = 1, \dots, \Lambda \tag{39}$$

$$\sum_{\lambda=1}^{\Lambda} \Delta_\lambda \le 1 \tag{40}$$

$$\delta_\lambda \ge 0 \;\;,\;\; \Delta_\lambda \in \{0,1\}\;, \quad \lambda = 1, \dots, \Lambda \tag{41}$$

where δ_λ and Δ_λ are required to obtain the piecewise linear representation of $F(z)$, and constant parameters ψ_λ, m_λ, and n_λ can be obtained from (42)-(44).

$$\psi_\lambda = \underline{z} + \lambda(1/\Lambda)(\overline{z} - \underline{z}) \quad , \lambda = 1, \dots, \Lambda \tag{42}$$

$$m_\lambda = [F(\psi_\lambda) - F(\psi_{\lambda-1})]/[\psi_\lambda - \psi_{\lambda-1}] \quad , \lambda = 1, \dots, \Lambda \tag{43}$$

$$n_\lambda = F(\psi_\lambda) - m_\lambda \psi_\lambda \quad , \lambda = 1, \dots, \Lambda \tag{44}$$

To shed light on the proposed linearization technique, the piecewise linear approximation of a typical non-linear function is illustrated in Fig. 12. The feasible range of the variable z is partitioned into Λ segments. Then, a line with a slope of m_λ and intercept of n_λ is considered corresponding to each segment λ. Finally, using the binary variables denoted by Δ_λ, only one of the lines is chosen to represent the non-linear function $F(z)$. Note that the parameter Λ determines the number of additional variables and constraints required to linearize $F(z)$. Therefore, the approximation error will obviously decrease as this parameter increases. Using the above-described linearization technique, the proposed CCED problem is now converted to an MILP-based model, which guarantees the solution optimality and computational tractability.

D. Solution Methodology

The detailed steps of the proposed solution methodology are as follows.

Step (1) **Initialization:** Set decision vector $\boldsymbol{x}$ on zero where $\boldsymbol{x} = [P_{t,i}, w_{t,j}, r_{t,i}^{UP}, r_{t,i}^{DN}, R_t^{UP}, R_t^{DN}, \delta_\lambda, \Delta_\lambda]$, $\Lambda = 10$, $CL^{UP} = CL^{DN} = 0.95$, $\mathrm{UB} = +\infty$, $\mathrm{LB} = -\infty$, and MILP gap tolerance $\varepsilon = 1\mathrm{e}-3$.

Step (2) **Receiving system data:** NG, NW, d_t, L_t^b, c_i^{UP}, c_i^{DN}, $\underline{P}_i$, $\overline{P}_i$, $\overline{\Delta P}_i^{UP}$, $\overline{\Delta P}_i^{DN}$, $\overline{r}_i^{UP}$, $\overline{r}_i^{DN}$, γ^{UP}, γ^{LS}, γ^{DN}, and γ^{WC}.

Step (3) **Modeling NCF:** Obtain A_q, A'_q, B_q, and B'_q of aggregate wind generation based on the wind power forecast values and CL^{UP} and CL^{DN} (Algorithm 3), and obtain $\widehat{EC}_t^{UP}$, $\widehat{EC}_t^{LS}$, $\widehat{EC}_t^{DN}$, and $\widehat{EC}_t^{WC}$ to create NCF as shown by (36).

Step (4) **Linearizing NCF:** linearize $C_{t,i}^{g}$, $\widehat{EC}_t^{UP}$, $\widehat{EC}_t^{LS}$, $\widehat{EC}_t^{DN}$, and $\widehat{EC}_t^{WC}$ simultaneously using piecewise linearization in (37)-(44).

Step (5) **Solving linearized NCF:** Minimize the linearized NCF with CPLEX (i.e., *cplexmilp*) subject to constraints (22)-(31) where $\mathbf{NCF} =$

$\sum_{t=1}^{T}\Delta t.\left(\sum_{i=1}^{NG} C_{t,i}^{g}+\sum_{i=1}^{NG} C_{t,i}^{r}+C_{t}^{dw}+\widehat{EC}_{t}^{UP}+\widehat{EC}_{t}^{LS}+\widehat{EC}_{t}^{DN}+\widehat{EC}_{t}^{WC}\right)$.

Step (6) **Updating cost coefficients of aggregate wind generation:** After a specific time period (e.g., one week), update the coefficients A_q, A'_q, B_q, and B'_q by receiving new wind power samples that lead to new wind power distribution $\hat{f}_t(\omega)$, then go to *Step (3)*.

V. Case Studies

A. Test System

To show the efficiency of the proposed approach, the widely used IEEE 118-bus test system with 54 CPPs is simulated in this study. The total base loads in the system considered over a 4-hour scheduling period are 3.6, 3.9, 4.1, and 4.2 GW. The developed MILP-based CCED model is solved by CPLEX 12.6.1 using MATLAB R2015a on a Corei7-6700 CPU@3.40 GHz personal computer with 16GB RAM.

B. Experimental Datasets and Wind Power Penetration Scenarios

Three different wind power datasets, introduced in Section II-E, are used to examine the proposed MILP-based CCED problem. Three penetration scenarios with different combinations of wind power datasets are considered in the system under study. **Case 1**- 150 MW wind power generation using WF2; **Case 2**- 167 MW wind generation using two different wind farms (WF2 and WF3); and **Case 3**- High penetration of wind power is assessed in this case with WF1, WF2, and WF3 with total capacity of 1630 MW. The correlation level among wind farms in Case 1 to Case 3 are not considered. To demonstrate the effect of correlation on total cost of the system, Case 4 and Case 5 are defined. **Case 4** is like Case 2 with three values $\rho = 0$, 0.50, and 0.95 as correlation coefficients. **Case 5** is like Case 3 considering two correlation matrices $\mathbb{R}_1$ and $\mathbb{R}_2$ shown below. Note that to construct wind power datasets with abovementioned correlation coefficients in Case 4 and Case 5, wind power time series WF1 to WF3 are checked and appropriate time lags are found in each time series to construct desired correlated time series.

$$\mathbb{R}_1=\begin{bmatrix}1.00 & 0.00 & 0.07\\ 0.00 & 1.00 & 0.06\\ 0.07 & 0.06 & 1.00\end{bmatrix}\qquad \mathbb{R}_2=\begin{bmatrix}1.00 & 0.95 & 0.90\\ 0.95 & 1.00 & 0.95\\ 0.90 & 0.95 & 1.00\end{bmatrix}$$

C. Simulation Results of the Proposed MILP-based CCED Problem

This section examines the proposed model using the IEEE 118-bus test system with Cases 1 to 5 with the proposed model. The results are compared with conventional approaches in which either an SLP optimization technique or TVD model (as a parametric distribution model) is used. In this study, c_i^{UP} and c_i^{DN} are considered to be \$15/MWh, and γ^{UP}, γ^{LS}, γ^{DN}, and γ^{WC} are set at \$120, \$200, \$60, and \$120/MWh, respectively. The generation of CPPs and wind farms as well as the system's required reserve are determined for the next 4-hour scheduling period with 10-min resolution. It is assumed that wind farms' forecast values change from 0.06 to 0.94 p.u. Tables IV, V, and VI show the value of different parts of the CCED cost function in (14) for Cases 1, 2, and 3, respectively. The results of the proposed MILP-based model (i.e., MILP-NCF-BKDR) are shown in the first numerical column. The second numerical column reflects the results of the approach, which includes NCF and BKDR while it is solved using SLP technique (i.e., SLP-NCF-BKDR). The third numerical column indicates the results of the CCED model comprised of the CCF in (14) and TVD model and solved by SLP technique (i.e., SLP-CCF-TVD).

The comparisons show that if the proposed NCF is linearized with the piecewise linearization technique, compared to SLP-NCF-BKDR, the developed MILP-based model can decrease the total cost of the system by \$985, \$1,147, and \$2,474 over just four hours for Cases 1 to 3, respectively. Compared with SLP-CCF-TVD, the reductions in total cost are, respectively, \$3,150, \$2,303, and \$6,154 for Cases 1 to 3 over four hours. A significant reduction in the system's total cost will occur over a year if power system operators use the proposed model for two reasons. First, the proposed model, based on wind power forecast values, incorporates accurate wind power distribution models and efficiently identifies four main areas of wind power distribution (Fig. 7) so that there is no miscalculation for upward reserve, load shedding, downward reserve, and wind curtailment costs. Second, the NCF is used that allows the system operators to convert the CCED problem to an MILP-based problem and efficiently solve it using powerful off-the-shelf solvers to obtain

TABLE IV
TOTAL COST OF THE IEEE 118-BUS TEST SYSTEM IN CASE 1

Cost (\$) (CL=95%)	MILP-NCF-BKDR	SLP-NCF-BKDR	SLP-CCF-TVD
EC^{UP}	3,668	3,725	3,731
EC^{LS}	204	171	193
EC^{DN}	1,093	1,041	1,082
EC^{WC}	233	337	396
C^{dw}	583	600	608
C^{r}	2,673	2,614	3,510
C^{g}	218,571	219,522	220,655
Total	**227,025**	**228,010**	**230,175**

TABLE V
TOTAL COST OF THE IEEE 118-BUS TEST SYSTEM IN CASE 2

Cost (\$) (CL=95%)	MILP-NCF-BKDR	SLP-NCF-BKDR	SLP-CCF-TVD
EC^{UP}	1,844	1,742	1,805
EC^{LS}	113	174	179
EC^{DN}	579	557	568
EC^{WC}	131	176	192
C^{dw}	646	654	679
C^{r}	1,219	1,353	1,397
C^{g}	218,079	219,102	220,094
Total	**222,611**	**223,758**	**224,914**

TABLE VI
TOTAL COST OF THE IEEE 118-BUS TEST SYSTEM IN CASE 3

Cost (\$) (CL=95%)	MILP-NCF-BKDR	SLP-NCF-BKDR	SLP-CCF-TVD
EC^{UP}	11,705	8,390	9,560
EC^{LS}	366	2,355	2,354
EC^{DN}	3,806	3,604	3,764
EC^{WC}	333	736	892
C^{dw}	6,243	6,409	6,580
C^{r}	5,970	7,243	7,435
C^{g}	178,000	180,160	181,992
Total	**206,423**	**208,897**	**212,577**

TABLE VII
TOTAL COST OF THE IEEE 118-BUS TEST SYSTEM IN CASE 4

CL=95% Base Load Coefficient=1		$\rho = 0$	$\rho = 0.5$	$\rho = 0.95$
MILP-NCF-BKDR	C^{g}	218,099	218,091	218,098
	C^{r}	**1,218**	**1,284**	**1,319**
	C^{dw}	643	645	644
	ΣEC	**2,708**	**2,772**	**2,840**
	Total	**222,668**	**222,792**	**222,901**
SLP-NCF-BKDR	C^{g}	219,090	219,093	219,068
	C^{r}	1,285	1,415	1293
	C^{dw}	657	657	660
	ΣEC	2,718	2,775	2,888
	Total	**223,750**	**223,940**	**223,909**

TABLE VIII
TOTAL COST OF THE IEEE 118-BUS TEST SYSTEM IN CASE 5

CL=95% Base Load Coefficient=1		$\mathbb{R}_1$	$\mathbb{R}_2$
MILP-NCF-BKDR	C^{g}	177,966	177,966
	C^{r}	**11,635**	**12,631**
	C^{dw}	6,249	6249
	ΣEC	**26,390**	**27,771**
	Total	**222,240**	**224,617**
SLP-NCF-BKDR	C^{g}	180,164	180,703
	C^{r}	11,635	12,780
	C^{dw}	6,408	6,324
	ΣEC	27,034	26,974
	Total	**225,242**	**226,783**

TABLE IX
COMPUTATION TIME OF CCED MODELS FOR IEEE 118-BUS TEST SYSTEM

CCED Model	MILP-NCF BKDR	SLP-NCF-BKDR	SLP-CCF-TVD
Average Time (sec.)	8.15	4.28	14.20

TABLE X
AVERAGE CONVERGENCE TIME IN THE PROPOSED MILP-BASED APPROACH

Λ \ MILP Gap	ε = 1e-3	ε = 5e-3	ε = 1e-2	ε = 5e-2
5	1.31s	1.27s	1.25s	1.26s
10	5.6s	5.4s	5.5s	5.6s

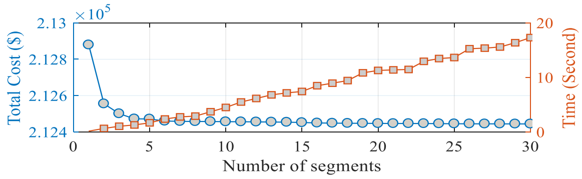

Fig. 13. Total cost and solution time of the proposed MILP-based CCED problem versus the number of linearization segments.

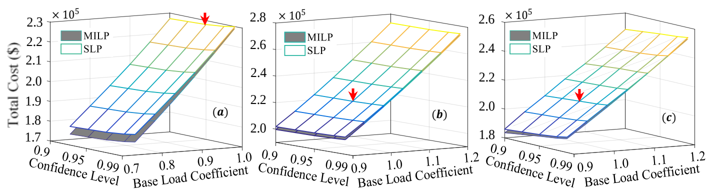

Fig. 14. Illustration of total cost hyperplane vs. confidence level and system load level for, (a) Case 1, (b) Case 2, and (c) Case 3.

the more optimal solution. For example, unlike the upward reserve and wind curtailment costs, the costs of load shedding and downward reserve in Case 1 obtained by MILP-NCF-BKDR are more than those obtained by SLP-CCF-TVD. However, the total cost of wind power generation and its uncertainty for the proposed approach is $5,781 while for the other two approaches are $5,874 and $6,010, respectively. The same interpretation can be made for Cases 2 and 3. In Case 2, the total costs of wind power generation for MILP-NCF-BKDR, SLP-NCF-BKDR, and SLP-CCF-TVD are $3,313, $3,303, and $3,423, respectively. These costs for Case 3 are higher at $22,453, $21,494, and $23,150, respectively. Although wind power related cost in the proposed model is more than other models in Cases 2 and 3, the generation and reserve costs of CPPs are less. Also, increasing wind power penetration, if appropriately managed, leads to less CPPs' generation cost. It is worth mentioning that if the chance constraints (27) are applied for each individual wind farm without considering the joint distribution of wind farms, the solution would be over conservative. In such a case, Case 2 and Case 3 result in $227,172 and $212,443 as total cost, respectively. The high accuracy of the piecewise linearization technique guarantees that the solution of the MILP-based model is the more optimal solution of the initial non-linear CCED problem. Tables VII and VIII examine the effect of correlation among wind farms on each part of total cost. The results of MILP-based model show that high levels of correlation necessitate more reserve cost, i.e., C^r and more expected cost of wind power misestimation, i.e., ΣEC, and the other costs, i.e., C^g and $C^{dw}$are almost unchanged. However, with the SLP-based model, such statement cannot be concluded because SLP-based model might not reach the optimal solution for different correlation levels. The computation time for three utilized CCED model is indicated in Table IX. Note that for the linearization purpose in the proposed MILP-based model, the number of segments and the MILP gap equal 15 and 1%, respectively. Table X reflects the effect of the number of linearization segments and MILP gap on the convergence of the proposed MILP-based algorithm. Also, Fig. 13 shows that, by increasing the number of segments Λ for linearization purposes, the accuracy of the MILP-based model increases, but it reaches a plateau after a certain value. Fig. 14 shows the total cost of the system versus total base load changes and different values for confidence level over the range [0.90, 0.99]. The total base load varies with predefined base load coefficients from 0.75 to 1 for Case 1 and from 0.9 to 1.2 for Case 2 and Case 3. The red arrows in Fig. 14 show the results presented in Tables IV to VI, which are for CL=95%, and the base load coefficient equals one. Also, Fig. 15 shows the performance of MILP-based and SLP-based CCED models with different values of CL and correlation level. The red arrows in Fig. 15 reflect the results in Table VII and Table VIII. The Figs. 14 and 15 indicate the superiority of the

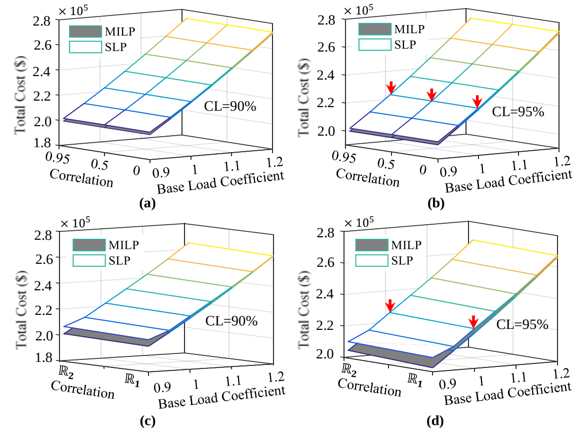

Fig. 15. Illustration of total cost hyperplane vs. correlation level and system load level, (a)-(b) Case 4, and (c)-(d) Case 5.

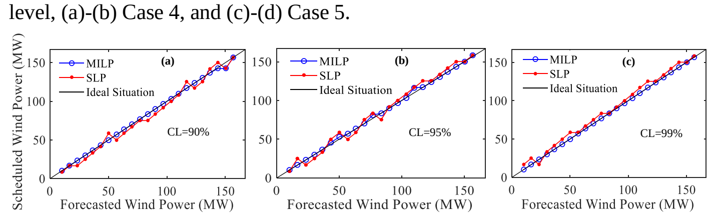

Fig. 16. Scheduled vs. forecasted wind power generation in Case 2.

proposed MILP-based model under all conditions. Fig. 16 shows the scheduled and forecast values in Case 2 for the proposed MILP-based and SLP-based models. Usually, with SLP-NCF-BKDR model, the scheduled wind power generation is lower than the corresponding forecast values for lower confidence levels (i.e., 90%) while for higher confidence levels (i.e., 99%) the scheduled wind power generation is greater than the forecast values. On the contrary, for all confidence levels in the proposed MILP-based model, the scheduled wind power generation is very close to the forecast values. The average values of RMSE for the proposed MILP-based model are 1.26, 0.87, and 0%, for 90, 95, and 99% confidence levels, respectively. In contrast, the average values of RMSE for the SLP-based model reach higher values of 2.97, 3.14, and 3.01%, respectively.

VI. CONCLUSION

This paper proposes an efficient wind power probability distribution modeling using sample moments of wind power data and BKDR technique. The proposed model shows high accuracy and low computational burden for practical applications. Also, an efficient methodology for obtaining an NCF is proposed to be able to convert the conventional non-linear CCED model to an MILP-based model using an accurate piecewise linearization technique. The proposed MILP-based CCED model is convex with respect to the continuous variables of the system and can effectively minimize the total cost. Moreover, the proposed CCED model enables power system operators to use both parametric and non-parametric models of wind power CDF. The NCF includes a set of cost coefficients which are stored in a database and calculated through CDF calculation before running CCED model. As a result, the solution process is computationally efficient and much closer to the global solution of the initial non-linear CCED problem. In addition, the proposed MILP-based model can consistently reflect the effect of WFs' correlation on the total reserve and wind power misestimation costs. Furthermore, because the nonlinearity of the CCED cost function increases proportional to wind power generation capacity, the proposed model is very efficient in high wind power penetration scenarios. Compared to the existing approaches, the proposed CCED model leads to a more optimal generation and reserve scheduling, thereby achieving a reasonable reduction in total system costs. As future works, in the proposed MILP-based CCED model, the uncertainty of solar generation and electricity load can also be efficiently considered. Without loss of generality, the proposed NCF and MILP-based CCED model can be formed after probability distribution modeling of correlated uncertain resources such as wind power, solar power, and electricity load. Moreover, as wind farms might have different levels of uncertainty, certain penalty factors and chance constraints might be defined for individual wind farms owning by different producers. Therefore, the required reserve for managing the underestimation and overestimation of each wind farm can be efficiently determined proportional to its level of uncertainty without calculating the aggregate wind power generation. In addition, the proposed MILP-based model might be adopted by look-ahead CCED problems using DRCC optimization approaches. In DRCC, instead of accurate distribution modeling, by defining an ambiguity set for wind power generation, a family of simple distributions are covered to compensate inaccurate distribution modeling.

References

[1] M. Doostizadeh *et al.*, “Energy and reserve scheduling under wind power uncertainty: An adjustable interval approach,” *IEEE Trans. Smart Grid*, vol. 7, no. 6, pp. 2943–2952, Nov. 2016.

[2] Z. S. Zhang *et al.*, “A versatile probability distribution model for wind power forecast errors and its application in economic dispatch,” *IEEE Trans. Power Syst.*, vol. 28, no. 3, pp. 3114–3125, Aug. 2013.

[3] C. Tang *et al.*, “Look-ahead economic dispatch with adjustable confidence interval based on a truncated versatile distribution model for wind power” *IEEE Trans. Power Syst.*, vol. 33, no. 2, pp. 1755–1767, Mar. 2018.

[4] Z. W. Wang, C. Shen, F. Liu, X. Y. Wu, C. C. Liu, F. Gao, "Chance-constrained economic dispatch with non-Gaussian correlated wind power uncertainty", *IEEE Trans. Power Syst.*, vol. 32, no. 6, Nov. 2017.

[5] C. Tang, *et al*., “A versatile mixture distribution and its application in economic dispatch with multiple wind farms,” *IEEE Trans. Sustain. Energy*, vol. PP, no. 99, pp. 1–1, 2017.

[6] Kenneth Bruninx and Erik Delarue, “A statistical description of the error on wind power forecasts for probabilistic reserve sizing,” *IEEE Trans. Sustain. Energy*, vol. 5, no. 3, pp. 995–1002, Jul. 2014.

[7] B. M. S. Hodge, *et al.*, “Characterizing and modeling wind power forecast errors from operational systems for use in wind integration planning studies,” *Wind Eng.*, vol. 36, no. 5, pp. 509–524, Oct. 2011.

[8] N. Zhang, C. Kang, Q. Xia, and J. Liang, “Modeling conditional forecast error for wind power in generation scheduling,” *IEEE Trans. Power Syst.*, vol. 29, no. 3, pp. 1316–1324, May 2014.

[9] F. Bouffard and F. D. Galiana, “Stochastic security for operations planning with significant wind power generation,” *IEEE Trans. Power Syst.*, vol. 23, no. 2, pp. 306–316, May 2008.

[10] H. Bludszuweit, J. A. Dominguez-Navarro, and A. Llombart, “Statistical analysis of wind power forecast error,” *IEEE Trans. Power Syst.*, vol. 23, no. 3, pp. 983–991, Aug. 2008.

[11] Y. Wang, N. Zhang, C. Kang, M. Miao, R. Shi, Q. Xia, "An efficient approach to power system uncertainty analysis with high-dimensional dependencies", *IEEE Trans. Power Syst.*, vol. 33, no. 3, May 2018.

[12] M. Cui, et al., “A data-driven methodology for probabilistic wind power ramp forecasting” *IEEE Trans. Smart Grid*, 2018, Early Access.

[13] M. Cui, et al. “Statistical representation of wind power ramps using a generalized gaussian mixture model” *IEEE Trans. Sust. Energy*, vol. 9, no. 1, pp. 261-272.

[14] M. Kaut, S. W. Wallace, "Evaluation of scenario-generation methods for stochastic programming", *Stochastic Program.*, vol. 3, no. 2, pp. 257-271, 2007.

[15] A. Papavasiliou, S. S. Oren, R. P. O’Neill, "Reserve requirements for wind power integration: A scenario-based stochastic programming framework", *IEEE Trans. Power Syst.*, vol. 26, no. 4, pp. 2197-2206, Nov. 2011.

[16] L. Yang, M. He, V. Vittal, J. Zhang, "Stochastic optimization-based economic dispatch and interruptible load management with increased wind penetration", *IEEE Trans. Smart Grid*, vol. 7, no. 2, pp. 730-739, Mar. 2016.

[17] M. Lubin, Y. Dvorkin, S. Backhaus, "A robust approach to chance constrained optimal power flow with renewable generation", *IEEE Trans. Power Syst.*, vol. 31, no. 5, pp. 3840-3849, Sep. 2016.

[18] Q. Wang, Y. Guan, J. Wang, "A chance-constrained two-stage stochastic program for unit commitment with uncertain wind power output", *IEEE Trans. Power Syst.*, vol. 27, no. 1, pp. 206-215, Feb. 2012.

[19] A. Zare, C. Y. Chung, J. Zhan, and S. O. Faried, "A distributionally robust chance-constrained MILP model for multistage distribution system planning with uncertain renewables and loads", *IEEE Trans. Power Systs.*, vol. 33, no. 5, pp. 5248-5262, 2018.

[20] C. Duan, W. Fang, L. Jiang, L. Yao, and J. Liu, "Distributionally robust chance-constrained approximate AC-OPF with Wasserstein metric", *IEEE Trans. Power Systs.*, vol. 33, no. 5, pp. 4924-4936, 2018.

[21] W. Wei, F. Liu, S. Mei, "Distributionally robust co-optimization of energy and reserve dispatch", *IEEE Trans. Sustain. Energy*, vol. 7, no. 1, pp. 289-300, Jan. 2016.

[22] L. Roald, S. Misra, T. Krause, G. Andersson, "Corrective control to handle forecast uncertainty: A chance constrained optimal power flow", *IEEE Trans. Power Syst.*, vol. 32, no. 2, pp. 1626-1637, Mar. 2017.

[23] L. Roald, G. Andersson, "Chance-constrained AC optimal power flow: Reformulations and efficient algorithms", *IEEE Trans. Power Syst.*, vol. 33, no. 3, pp. 2906-2918, May 2018.

[24] R. Jiang, Y. Guan, "Data-driven chance constrained stochastic program", *Math. Program.*, vol. 158, pp. 291-327, 2016.

[25] A. Lorca, X. A. Sun, "Adaptive robust optimization with dynamic uncertainty sets for multi-period economic dispatch under significant wind", *IEEE Trans. Power Syst.*, vol. 30, no. 4, pp. 1702-1713, Jul. 2015.

[26] Z. Li, W. Wu, B. Zhang, B. Wang, "Adjustable robust real-time power dispatch with large-scale wind power integration", *IEEE Trans. Sustain. Energy*, vol. 6, no. 2, pp. 357-368, Apr. 2015.

[27] W. Wu, J. Chen, B. Zhang, H. Sun, "A robust wind power optimization method for look-ahead power dispatch", *IEEE Trans. Sustain. Energy*, vol. 5, no. 2, pp. 507-515, Apr. 2014.

[28] Y. Wang, Q. Xia, C. Kang, "Unit commitment with volatile node injections by using interval optimization", *IEEE Trans. Power Syst.*, vol. 26, no. 3, pp. 1705-1713, Aug. 2011.

[29] X. Dui, G. Zhu, and L. Yao, "Two-stage optimization of battery energy storage capacity to decrease wind power curtailment in grid-connected wind farms," *IEEE Trans. Power Syst.*, vol. 33, no. 3, pp. 3296–3305, May 2018.

[30] L. Che, et al., “Intra-interval security based dispatch for power systems with high wind penetration,” *IEEE Trans. Power Syst*., 2018 , Early Access.

[31] E. Du et al., "Managing wind power uncertainty through strategic reserve purchasing", *IEEE Trans. Power Syst.*, vol. 32, no. 4, pp. 2547-2559, Jul. 2017.

[32] N. Zhang, et al., “A convex model of risk-based unit commitment for day-ahead market clearing considering wind power uncertainty,” *IEEE Trans. Power Syst*., vol. 30, no. 3, May 2015.

[33] P. N. Gavriliadis and G. A. Athanassoulis, “The truncated Stieltjes moment problem solved by using kernel density functions,” *Journal of Computational and Applied Mathematics*, 236 (2012), 4193-4213.

[34] G. A. Athanassoulis and P. N. Gavriliadis, “The truncated Hausdorff moment problem solved by using kernel density functions,” *Probabilistic Engineering Mechanics*, 17(2002), 273-291.

[35] J. Hetzer, D. C. Yu, K. Bhattarai, "An economic dispatch model incorporating wind power", *IEEE Trans. Energy Convers.*, vol. 23, no. 2, pp. 603-611, Jun. 2008.

[36] https://www.aeso.ca/market/market-and-system-reporting/data-requests/.

[37] http://www.sotaventogalicia.com/en/real-time-data/historical.

[38] P. Kall, and J. Meyer, “Stochastic Linear Programming, Models, Theory, and Computation,” Springer, 2005.

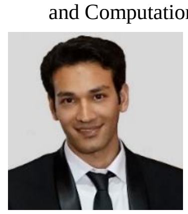

Benyamin Khorramdel (S’14) is currently working toward the Ph.D. degree at the University of Saskatchewan, Saskatoon, SK, Canada. He is now a visiting researcher at Powertech Labs, BC, Canada. His current research interests include machine learning, wind power forecasting, uncertainty modeling, optimization, and operation of renewable energy integrated power systems.

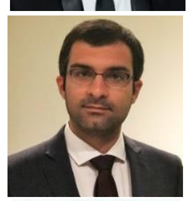

Alireza Zare (S’14) received the Ph.D. degree in electrical engineering from University of Saskatchewan, Saskatchewan, Canada, in 2018. He is currently working as an engineer-in-training at SaskPower, Regina, Canada. His research interests include transmission system planning, distribution system planning, renewable and distributed energy resources, microgrids, energy management of electric vehicles, and smart grid.

C. Y. Chung (M’01-SM’07-F’16) is currently a Professor, the NSERC/SaskPower (Senior) Industrial Research Chair in Smart Grid Technologies, and the SaskPower Chair in Power Systems Engineering in the Department of Electrical and Computer Engineering at the University of Saskatchewan, Saskatoon, SK, Canada. His research interests include smart grid technologies, renewable energy, power system stability/control, planning and operation, computational intelligence applications, power markets and electric vehicle charging. Dr. Chung is an Editor of *IEEE Transactions on Power Systems* and *IEEE Transactions on Sustainable Energy*.

Panagiotis Gavriliadis received Ph.D. degree in Marine Hydrodynamics from the National Technical University of Athens (NTUA), Athens, Greece in 2006. He is currently a laboratory teaching staff in the Department of Naval Architecture and Marine Engineering at the NTUA, Greece. His research interests include inverse problems and stochastic modelling.